INORGANIC CHEMISTRY
FRONTIERS

RESEARCH ARTICLE

View Article Online
View Journal | View Issue

Cite this: *Inorg. Chem. Front.*, 2024, **11**, 853

Cooperativity in luminescent heterobimetallic diphosphine-ß-diketiminate complexes†

Frederic Krätschmer,[a] Xiaofei Sun,[a] David Frick,[a] Christina Zovko,[a] Wim Klopper[b] and Peter W. Roesky *[a]

Received 30th August 2023,
Accepted 5th December 2023

DOI: 10.1039/d3qi01740k

rsc.li/frontiers-inorganic

The bis(phosphine)-functionalized β-diketiminate ligand $[HC\{(CH_3)C\}_2\{(o\text{-}[P(C_6H_5)_2]_2C_6H_4)N\}_2]^-$ (PNac) was used for the synthesis of luminescent closed-shell bimetallic complexes. The PNNP pocket combining both soft and hard donor sites can act as an orthogonal ligand scaffold to selectively coordinate two different metal ions. Deprotonation and subsequent salt elimination with [AuCl(tht)] (tht = tetrahydrothiophene) or AgI yielded the mononuclear complexes [PNacAu] (**1**) or [PNacAg] (**2**), respectively. The Au^I ion is linearly coordinated by the two phosphines, forming a 12-membered metalla-macrocycle with an empty ß-diketiminate pocket available for complexation of hard d^{10} metal ions (Zn^{II}, Cd^{II}, and Hg^{II}). According to this synthetic protocol, a series of heterobimetallic complexes were isolated. The complexation of the second metal ion in close spatial proximity has led to drastic changes in the photophysical properties. For further studies and understanding, quantum chemical calculations were performed.

Introduction

Cooperative effects in bi- and multimetallic complexes are of much interest and are known for their applications in enhancing catalytic properties, increasing chemical reactivities and tuning photophysical properties.[1–3] The presence of two metal centres in homo- or heterobimetallic systems can result in a significant modification of the individual properties or lead to novel characteristics that are unattainable in monometallic compounds.[4–8] Examples are metal–metal bond formation, redox processes, and changes in polarity or distance.[9–11] The most iconic example of cooperativity is found in catalysis. Two metals can synergise in a multistep process as multi-catalysts to promote tandem processes, for example, the Pd or Rh triazolyldiylidene complexes of Peris *et al.*[12–16] Several types of model complexes can be considered as bimetallic cooperative systems (Fig. 1). The two metal centres can have direct contact through a metal–metal bond (A) or have some distinct metallophilic interactions (B) but can also be spatially separated by a linker (C). By selection of a suitable ligand system the two metal atoms can also be brought in close proximity to each other (Fig. 1D).[2,6,11,17–21] Even with large metal–metal separation cooperative effects have been observed, for example, in the dihydroalkoxylation of an alkyne diol with bimetallic Ir^I and Rh^I complexes.[22–25] However, cooperative effects are also of great significance in adjusting the luminescence properties of multimetallic complexes. It is well established that complexes, which feature metallophilic contacts, often show rich photophysical properties that are influenced by the multimetallic scaffold.[26–28] In general, heavy atoms such as gold allow, due to enhanced spin–orbit coupling (heavy metal effect), efficient intersystem crossing (ISC),[29] which results in predominantly phosphorescence with emission decay times typically in the microsecond range.[27] Changing the metal–metal distances and the nature of the metals involved allows for tuning of the photoluminescence properties, which is of potential interest for applications in fields ranging from OLED design and sensor technology to tumour markers.[30–32] The specific coordination of two different metal ions within the same ligand framework is synthetically challenging. For these purposes, the so-called orthogonal ligand systems need to be designed and synthesised.[33,34] To achieve a selective coordination of different metal ions in a bifunctional ligand, Pearson's principle of hard and soft acids and bases (HSAB) can be considered.[35,36] In particular, coinage metals are known for their different behaviour towards hard and soft coordination sites.[37–41] In this manner, gold as the "softest" cation prefers "soft" donors, while copper as a "hard" metal ion has great affinity for "hard" donors. The bis(diphenyl) phosphine-functionalised β-diketiminato ligand system $[HC\{(CH_3)C\}_2\{(o\text{-}[P(C_6H_5)_2]_2C_6H_4)N\}_2]^-$ (PNac) might be a perfect

[a]*Institute of Inorganic Chemistry, Karlsruhe Institute of Technology (KIT), Engesserstr. 15, 76131 Karlsruhe, Germany. E-mail: roesky@kit.edu*
[b]*Institute of Physical Chemistry, Karlsruhe Institute of Technology (KIT), Fritz-Haber-Weg 2, 76131 Karlsruhe, Germany*

†Electronic supplementary information (ESI) available: Synthetic protocols; NMR, IR, Raman, and UV/Vis spectra; PL data, SCRD data, and quantum chemical calculations. CCDC 2264854–2264861. For ESI and crystallographic data in CIF or other electronic format see DOI: https://doi.org/10.1039/d3qi01740k

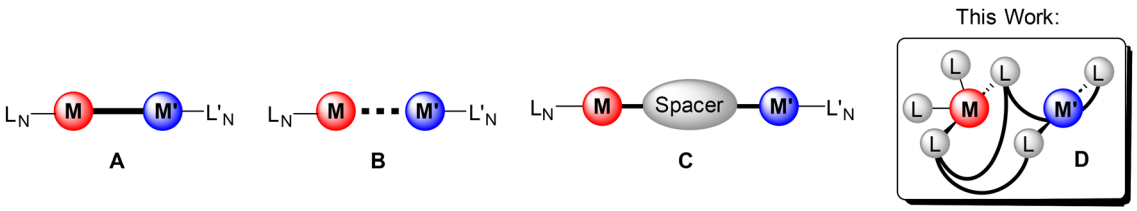

Fig. 1 Bimetallic systems: with metal–metal bond interaction (A), metallophilic interaction (B), bridged bimetallic compounds (C), and spatial proximity of metal centres driven by rigid ligands (this work) (D).

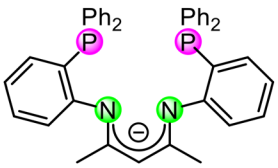

Fig. 2 Monoanionic PNac as an orthogonal ligand with hard nitrogen (green) and soft phosphorous (pink) donor sites.[42–44]

candidate to achieve heterobimetallic systems (Fig. 2). A wide range of mononuclear compounds with different coordination modes has been achieved.[42–44] Herein, we expand the coordination chemistry of the PNac ligand and provide a synthetic protocol for heterobimetallic compounds with coinage- and group 12 metals. Compared to monometallic species, introducing the second metal in close spatial proximity led to a significant enhancement of their photoluminescence properties (Fig. 1D).

Results and discussion

Herein, we showcase the highly selective assembly of the desired heterobimetallic species in either one-pot synthesis or in a stepwise approach starting from mononuclear Ag^{I} or Au^{I} complexes. Therefore, the synthesis of these mononuclear compounds, which were subsequently used as precursors and as benchmark compounds for the luminescence measurements, is discussed first.[45]

Mononuclear compounds[45]

The mononuclear compounds [PNacAu] (**1**) and [PNacAg] (**2**) were synthesised conveniently by the salt elimination reaction. The deprotonation of PNac-H in tetrahydrofuran (THF) with a potassium base and subsequent addition of coinage metal halides ([AuCl(tht)] or AgI) yielded the desired compounds **1** and **2**, respectively (Scheme 1). Single crystals of the respective complexes suitable for X-ray diffraction analysis were obtained by layering the THF solution with *n*-pentane.

Compound **1** forms a 12-membered metalla-macrocycle in the solid-state (Fig. 3, left). The Au^{I} ion is exclusively coordinated to two phosphine moieties in a linear fashion with a P1–Au–P2 angle of 169.12(6)°. This is slightly more acute than the bond angle (175.08(5)°) in the ionic species [PNac-H-Au][ClO_4].[43] Due to the formation of the metalla-macrocycles a kind of zwitterionic charge-separated species is formed, in which the β-diketiminato backbone is formally negatively charged, while the Au^{I} atom is the positive part. A similar "charge-separated" structure was observed for the related binuclear Au^{I} complex [dpfam$_2$Au$_2$] (dpfam = *N*,*N*′-bis[(2-diphenylphosphino)phenyl]-formamidinate).[39] The distances

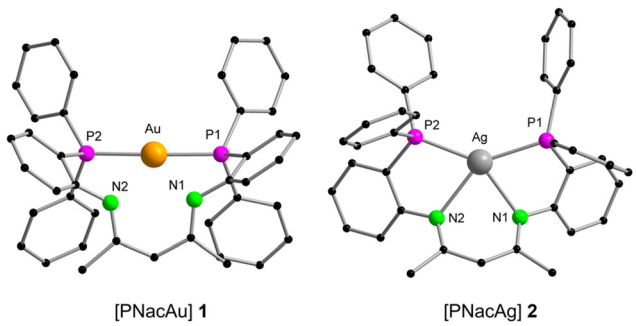

[PNacAu] **1** [PNacAg] **2**

Fig. 3 Molecular structures of [PNacAu] **1** and [PNacAg] **2** in the solid state. Hydrogen atoms are omitted for clarity. Selected distances [Å] and angles [°]: **1**: P1–Au 2.2909(15), P2–Au 2.2881(15); P1–Au–P2 169.12(6); **2**: P1–Ag 2.4040(5), P2–Ag 2.4254(5), N1–Ag 2.4371(14), N2–Ag 2.4749 (14); P1–Ag–P2 140.78(2), N1–Ag–N2 72.04(5).

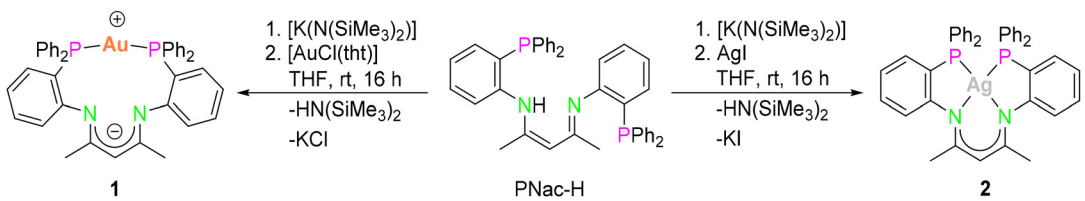

Scheme 1 Synthesis of the mononuclear compounds [PNacAu] (**1**) and [PNacAg] (**2**) (tht = tetrahydrothiophene).

between the Au^I centre and the N atoms are 2.858(5) Å (Au–N1) and 2.866(5) Å (Au–N2), which are beyond typical Au–N bond distances (2.03 Å to 2.38 Å),[46,47] hence ruling out a bonding interaction. The C–N (1.305(8) Å and 1.311(8) Å) and C–C bonds (1.405(9) Å and 1.397(9) Å) in the β-diketiminato backbone show bond lengths between single and double bonds, indicating the delocalisation of the negative charge.

In the $^{31}P\{^1H\}$ NMR spectrum, one singlet resonance was detected for the phosphorous atoms at 28.6 ppm. This peak is significantly downfield-shifted compared with the free ligand (−14.5 ppm), but slightly upfield-shifted from that of [PNac-H-Au][ClO_4] (34.5 ppm),[43] indicating a symmetric arrangement of the two phosphine moieties in solution.[48]

The molecular structure of **2** in the solid state deviates from that of complex **1** (Fig. 3, right). Instead of the Au^I cation in **1** being linearly coordinated by two phosphines, the Ag^I cation in **2** is tetracoordinated by both the two nitrogen atoms from the β-diketiminato and the two phosphine moieties, resulting in a distorted square planar coordination mode, thus being similar to the previously published [PNacCu] (**9**).[43] The Ag–N bond lengths (2.4371(14) Å (Ag–N1) and 2.4749(14) Å (Ag-N2)) are slightly elongated compared with those found in the bis (amidinate) Ag^I species [dpfam$_2$Ag$_2$] (2.302(2) Å and 2.453(2) Å).[39] The Ag^I coordination mode in complex **2** differs from that in the ionic complex [PNac-H-Ag][BF_4],[43] in which the Ag^I ion is linearly coordinated by both phosphines. This distinct coordination of the central metal atom in **1** and **2** is in agreement with the "softer" nature of Au^I compared to Ag^I.[43] The $^{31}P\{^1H\}$ NMR spectrum of complex **2** exhibits two doublets at −10.7 ppm, originating from the coupling of the ^{31}P nucleus with ^{107}Ag and ^{109}Ag ($^1J_{P,^{107}Ag}$ = 391.7 Hz, $^1J_{P,^{109}Ag}$ = 452.2 Hz). The observed signal is high-field-shifted compared to [PNacAu] (**1**) as well as [PNac-H-Ag][BF_4] (1.2 ppm).[43]

Bimetallic compounds[45]

After having synthesised the monometallic complexes **1** and **2**, we aimed for access to bimetallic group 11/group 11 and group 11/group 12 complexes with d^{10} configuration. The aim was to study d^{10}/d^{10} interactions and cooperative effects of various metal combinations within the PNac scaffold. Depending on the corresponding metal precursor, different synthetic pathways were followed.

To obtain bimetallic complexes of the general formula of [PNacAu[M]] (**3**: [M] = CuI; **4**: [M] = $ZnCl_2$), the metal salts CuI or $ZnCl_2$ were added to a mixture of PNac-H and [Au(C_6F_5)(tht)] in THF (Scheme 2, *route A*). This route proceeds *via* a remarkable and previously not observed cooperative activation of PNac-H. Earlier reports on the reaction of PNac-H with just [M(C_6F_5)(L)] (M = Au^I, Ag^I) did not result in a deprotonation of the ligand. Instead, the addition of two equivalents of [Au(C_6F_5)(tht)] to PNac-H led to the formation of the neutral compound [PNac-H-(AuC_6F_5)$_2$].[43] Only by addition of another metal halide did deprotonation and coordination of both metal ions occur.

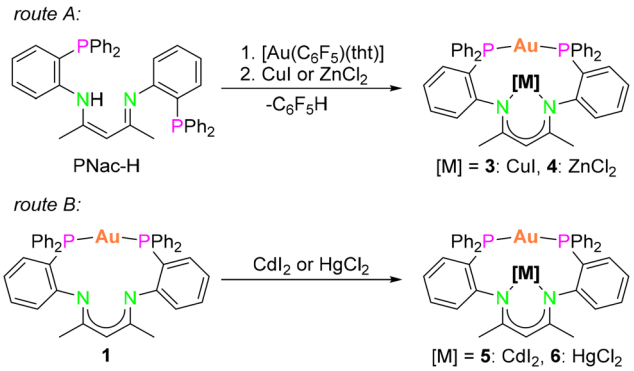

Scheme 2 Synthesis of bimetallic compounds **3**–**6**.

However, if a similar synthetic route was employed for CdI_2, the ionic species [PNac-H-Au][CdI_3(thf)$_2$] and [$CdIC_6F_5$] were formed. In comparison, addition of $HgCl_2$ to PNac-H and [Au(C_6F_5)(tht)] led to decomposition. Therefore, a second synthetic route (Scheme 2, *route B*) was developed for the access of bimetallic Au^I/Cd^{II} and Au^I/Hg^{II} complexes. In the mononuclear Au^I complex **1**, which forms a 12-membered metalla-macrocycle, the two N atoms remain uncoordinated. Using complex **1** as a precursor, the second metal ion could be encapsulated straightforwardly within the metalla-macrocycle by reacting the metal halides CdI_2 or $HgCl_2$ with **1** in an equimolar ratio in THF.

After filtration and layering the THF solution with *n*-pentane, single crystals of the bimetallic complexes [PNacAuCdI$_2$] (**5**) and [PNacAuHgCl$_2$] (**6**) were obtained, respectively. Therefore, complex **1** is a necessary building precursor for synthesising [PNacAu[M]] ([M] = CdI_2 (**5**) and $HgCl_2$ (**6**)). In addition, the bimetallic Au^I/Cu^I and Au^I/Zn^{II} complexes **3** and **4** could also be synthesised *via* the second route starting from the monometallic Au^I species **1**.

In [PNacAuCuI] (**3**) the Cu^I ion is trigonal planar coordinated by the two nitrogen atoms (N1 and N2) and iodide (Fig. 4). The P1–Au–P2 angle of 169.47(12)° is comparable with that in **1**, showing that the geometry of the Au^I atom is unaffected by the Cu^I ion. Additionally, the short intermetallic distance of 2.634(2) Å demonstrates that the PNac ligand is indeed able to enforce close spatial proximity. The distance is shorter than in other conventionally known literature examples (2.7 Å–3.0 Å).[38,49,50] The resonance in the $^{31}P\{^1H\}$ NMR spectrum at 27.1 ppm is only marginally shifted compared to the mononuclear Au^I complex **1** (28.6 ppm). The NMR spectra of **3** show persistent peaks of some decomposition products. In [PNacAuZnCl$_2$] (**4**) the Zn^{II} ion is tetrahedrally coordinated by two nitrogen atoms and two chlorides while the Au^I ion remains linearly coordinated with the P1–Au1–P2 angle being 169.01(4)° (Fig. 4). The $Au^I\cdots Zn^{II}$ distance of 3.2088(5) Å is much longer than for the $Au^I\cdots Cu^I$ distance in **3**. However, the ionic radius of Zn^{II} (0.60 Å) is comparable to that of Cu^I (0.46 Å),[51] leading to the conclusion that the ligand cannot bring Au^I and Zn^{II} in the same close proximity as Au^I and Cu^I.

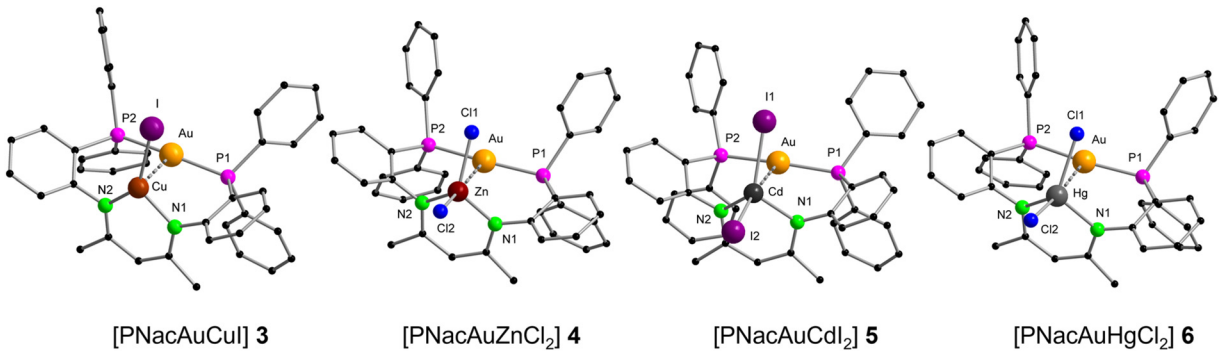

Fig. 4 Molecular structures of [PNacAuCuI] (**3**), [PNacAuZnCl$_2$] (**4**) [PNacAuCdI$_2$] (**5**) and [PNacAuHgCl$_2$] (**6**) in the solid-state. Hydrogen atoms are omitted for clarity. Selected distances [Å] and angles [°]: **3**: Au···Cu 2.634(2), P1–Au 2.293(3), P2–Au 2.290(3), N1–Cu 1.948(11), N2–Cu 1970(12), I-Cu 2.46(2); P1–Au–P2 169.47(12), N1–Cu–N2 95.6(5); **4**: Au···Zn 3.2088(5), P1–Au 2.3019(11), P2–Au 2.3009(12), N1–Zn 2.001(4), N2–Zn 2.003(4), Cl1–Zn 2.2641(12), Cl2–Zn 2.2536(13); P1–Au–P2 169.01(4), N1–Zn–N2 93.46(15); **5**: Au···Cd 3.3942(4), P–Au 2.3139(9), N–Cd 2.227(3), I–Cd 2.7253 (4); P–Au–P′ 167.68(5), N–Cd–N′ 84.41(13); **6**: Au···Hg 3.2417(2), P1–Au 2.2968(9), P2–Au 2.2968(9), N1–Hg 2.251(3), N2–Hg 2.255(3), Cl1–Hg 2.4589(9), Cl2–Hg 2.4160(10); P1–Au–P2 167.38(3), N1–Hg–N2 84.80(10).

The molecular structures of the complexes with the heavier group 12 homologues [PNacAuCdI$_2$] (**5**) and [PNacAuHgCl$_2$] (**6**) resemble that of **4** and thus will not be discussed in detail (Fig. 4). The Au^{I}···M^{II} distances rise from Zn^{II} over Hg^{II} to Cd^{II} (3.2088(5) Å over 3.2417(2) Å to 3.3942(4) Å) despite the larger ionic radius of Hg^{II}.[51] The Au^{I}···Hg^{II} distance is still slightly longer than that in literature known compounds.[52–58] It is remarkable that the computed values (*vide infra*) rise from Zn^{II} over Cd^{II} to Hg^{II}, which is in line with the ionic radii. The ^{31}P{^{1}H} NMR signals of the three compounds are **4**: 25.7 ppm, **5**: 27.4 ppm and **6**: 27.4 ppm, and thus the Zn^{II} compound shifts the furthest into the high field, compared to **1**.

The ^{113}Cd NMR spectrum of compound **5** revealed a resonance at −273.1 ppm, and additionally the ^{1}H NMR spectrum shows satellite peaks arising from the $^{4}J_{H,^{111/113}Cd}$ coupling (1.5 Hz) with the C$H_{ß\text{-diketiminate}}$ proton (4.3 ppm) and a $^{3}J_{C,^{111/113}Cd}$ coupling (4.2 Hz) with the CH_3 ^{13}C nucleus (22.3 ppm) in the ^{13}C{^{1}H,^{31}P} NMR spectrum. For **5**, a $^{4}J_{H,^{119}Hg}$ coupling (5.5 Hz) is visible for the C$H_{ß\text{-diketiminate}}$ proton (4.24 ppm).

The synthesis of the bimetallic Ag^{I} compounds [PNacAgZnCl$_2$] (**7**) and [PNacAgCdI$_2$] (**8**) (Scheme 3) can be achieved in a similar fashion to that of compounds **3** and **4** stated above (Scheme 2, *route A*). Here the reaction of PNac-H with [Ag(C$_6$F$_5$)(MeCN)] and CdI$_2$ leads to the formation of the desired product. Again, the C$_6$F$_5$ group acts as a base to deprotonate PNac-H. In addition, compounds **7** and **8** can also be synthesised starting with **2** in the same manner as shown in Scheme 2, route B. This showcased that both monometallic compounds **1** and **2** are capable precursors for the synthesis of all bimetallic compounds **3**–**8**. Unfortunately, the reaction with HgCl$_2$ led to decomposition using both synthetic approaches. A bimetallic Ag^{I}/Cu^{I} compound, which is isostructural to the Au^{I}/Cu^{I} complex **3** could not be synthesised and several attempts have been made but only the mononuclear copper species [PNacCu] (**9**) could be identified as a product.[43] In general, with the coordination of the second metal, a change in the coordination sphere of the Ag^{I} ion compared to the monometallic species **2** goes along, which may be one reason for the lower stability of the target complexes compared to the analogue Au^{I} compounds **3**–**6**. The structures of the Ag^{I}/Zn^{II} complex **7** and the Ag^{I}/Cd^{II} complex **8** resemble those of the Au^{I} compounds **4**, **5** and **6**. The Ag^{I}···Zn^{II} distance is 3.0941(7) Å, while Ag^{I}···Cd^{II} (3.2077(5) Å) is slightly longer (Fig. 5).

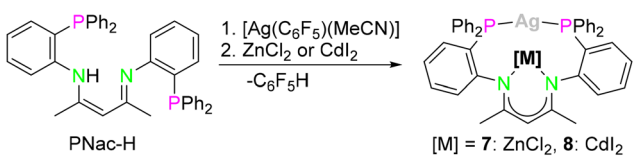

Scheme 3 Synthesis of bimetallic compounds [PNacAgZnCl$_2$] (**7**) and [PNacAgCdI$_2$] (**8**).

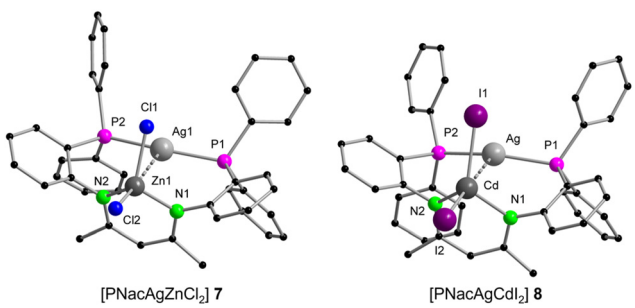

Fig. 5 Molecular structures of [PNacAgZnCl$_2$] (**7**) and [PNacAgCdI$_2$] (**8**) in the solid state. Hydrogen atoms are omitted for clarity. Compound **7** crystallises with two molecules in the asymmetric unit with similar metric data. Only one is described here. Selected distances [Å] and angles [°]: **7**: Ag1···Zn1 3.0941(7), P1–Ag1 2.4054(12), P2–Ag1 2.3984(12), N1–Zn1 2.009(4), N2–Zn1 2.009(4), Cl1–Zn1 2.2138(15), Cl2–Zn1 2.2776 (14); P1–Ag1–P2 160.97(4), N1–Zn1–N2 92.9(2); **8**: Ag···Cd 3.2077(5), P1–Ag 2.4282(12), P2–Ag 2.4271(12), N1–Cd 2.233(4), N2–Cd 2.248(4), I1–Cd 2.7502(5), I2–Cd 2.6841(5); P1–Ag–P2 154.76(4), N1–Cd–N2 83.82(13).

The resonances in the $^{31}P\{^{1}H\}$ NMR spectra in both compounds appear as two doublets at −2.3 ppm, which are slightly downfield shifted from the monometallic species **2** (−10.7 ppm). The coupling constants are $^{1}J_{P,^{107}Ag}$ = 496.6 Hz, $^{1}J_{P,^{109}Ag}$ = 572.8 Hz for **7** and $^{1}J_{P,^{107}Ag}$ = 470.3 Hz, $^{1}J_{P,^{109}Ag}$ = 543.3 Hz for **8**, which are larger than in compound **2** and are in the same range compared to literature known compounds.[43] In the ^{1}H NMR spectrum of the Ag^{I}/Cd^{II} complex **8**, satellites were found with a $^{4}J_{H,^{111/113}Cd}$ coupling (2.0 Hz) for the C*H* proton of the ß-diketiminato ligand (4.27 ppm). Accordingly, in the $^{13}C\{^{1}H,^{31}P\}$ NMR spectrum, the $C^{q}_{ß\text{-diketiminate}}$ (170.8 ppm), *C*H (95.9 ppm) and CH_3 (23.9 ppm) resonances display $^{111}Cd/^{113}Cd$ satellites with coupling constants of ^{2}J = 2.1 Hz, ^{3}J = 11.4 Hz and ^{3}J = 4.1 Hz. The signal in the ^{113}Cd NMR is slightly shifted compared to the Au^{I}/Cd^{II} complex **5** (−273.1 ppm) and shows a singlet resonance at −286.1 ppm. No coupling to $^{107/109}Ag$ could be detected.

Photoluminescence properties

The mono- and bimetallic compounds **1**–**8** as well as the previously reported potassium salt [PNacK] were investigated in terms of their photoluminescence behaviour in the solid state.[59] The beige to orange solids show luminescence behaviour at room temperature (293 K) and low temperature (77 K), emitting light in the range of yellow to orange and blue to green (Fig. 7 and 8 (right)). Interestingly the Raman spectra of the monometallic compounds **1** and **2** exclusively show broad Raman fluorescence (Fig. S35 and S36†). The photoluminescence (PL) spectrum of [PNacK] is depicted in Fig. 6, those of the Au^{I} containing compounds **1**, **3**–**6** are depicted in Fig. 7 and those of the Ag^{I} containing compounds are depicted in Fig. 8.

The spectra of [PNacK], **1** and **2** are quite similar showing excitation wavelengths of 490–540 nm and emissions around 560–620 nm. While the potassium salt shows fast fluorescence decay with a lifetime of 4 ns the processes in **1** and **2** are of phosphorescent nature with a lifetime of 566 µs for **1**. In contrast compound **2** shows a longer lifetime at room temperature than at 77 K with 67 µs. The phosphorescence decay can be attributed to the heavy atom effect. Note that the previously published mononuclear compound [PNacCu] (**9**) shows no significant photoluminescence properties.[43] The comparison of compounds **1** and **3** shows a broad emission maximum at 620 nm (at 77 K) for both, respectively, with a blueshift to 575 nm and 590 nm by increasing the temperature to 293 K. For compound **1** the NIR emission spectrum shows tailing of the curve until 1100 nm (see ESI Fig. S53†). Group 12 containing compounds **4**–**6** feature a redshift in their emission with increasing molecular weight with maxima at 495 nm, 505 nm and 580 nm, and therefore the Au^{I}/Hg^{II} complex **6** displays the broadest band. At elevated temperatures this trend is more distinctive due to a blueshift for Zn^{II} compound **4** and a redshift for **6**, while the emission maximum remains unchanged for **5**. The excitation spectra of compounds **1** and **6** show weak absorption in the UV region, but relatively broad bands around 500 nm and 480 nm, and therefore the Hg^{II} ion shows a weaker effect on the intraligand (IL) photoluminescence process of the ß-diketiminate scaffold than its lighter homologues. The metallophilic interaction between Au^{I} and Cu^{I} leads to enhanced emission at room temperature, which may be the result of a LMMCT (ligand to metal–metal charge transfer), and in the excitation spectra an onset at 500 nm (77 K) or 550 nm (293 K) ranging in the UV region is seen (Table 1).

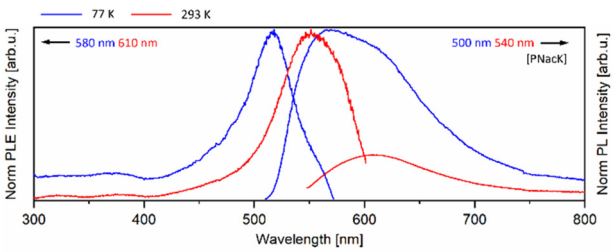

Fig. 6 Solid-state photoluminescence emission (PL) and excitation (PLE) spectra of [PNacK] at 77 K (blue) and 293 K (red).

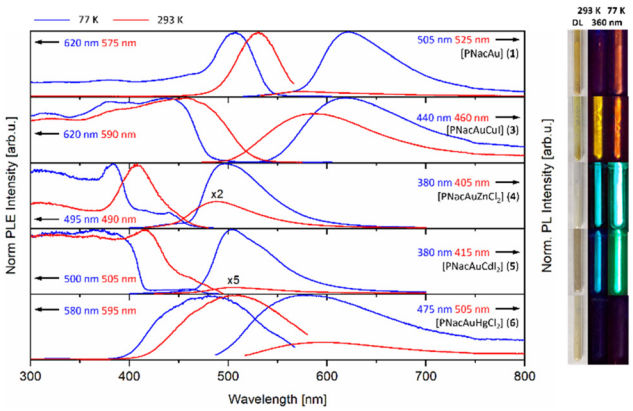

Fig. 7 Solid-state photoluminescence emission (PL) and excitation (PLE) spectra of Au^{I} compounds **1**, **3**–**6** at 77 K (blue) and 293 K (red). Pictures of the compounds at daylight (DL) (left), under 360 nm UV light (middle) at 293 K, and under 360 nm UV light at 77 K (right).

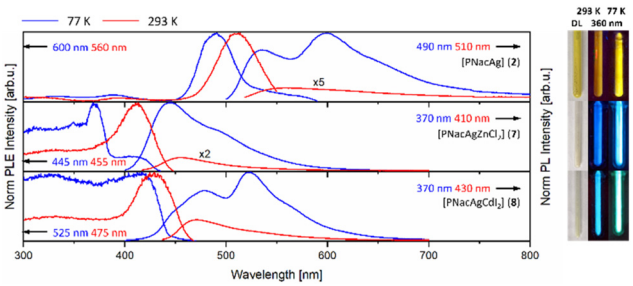

Fig. 8 Solid-state photoluminescence emission (PL) and excitation (PLE) spectra of Ag^{I} compounds **2**, **7** and **8** at 77 K (blue) and 293 K (red). Pictures of the compounds at daylight (DL) (left), under 360 nm UV light (middle) at 293 K, and under 360 nm UV light at 77 K (right).

Table 1 Experimental data of the PLE and PL spectra of [PNacK] and compounds **1–8**

	$\lambda_{max,\ exc}$ [nm]		$\lambda_{max,\ em}$ [nm]	
	77 K	293 K	77 K	293 K
1: [PNacK]	500	540	580	610
1: [PNacAu]	505	525	620	575
2: [PNacAg]	490	510	600	560
3: [PNacAuCu]	440	460	620	590
4: [PNacAuZn]	380	410	495	490
5: [PNacAuCd]	375	415	505	505
6: [PNacAuHg]	480	510	580	595
7: [PNacAgZn]	370	410	445	455
8: [PNacAgCd]	420	430	525	470

The coordination of the second metal (Zn^{II} and Cd^{II}) in the same ligand framework with Au^{I} leads to a bright blue emission at room temperature. For all compounds depicted in Fig. 7 the PLE onsets are redshifted with elevated temperatures. PL spectra of the Ag^{I} containing compounds **2**, **7** and **8** are shown in Fig. 8. In contrast to the monometallic Au^{I} compound **1**, complex **2** features two distinct maxima in the PL emission spectra at 535 nm and 600 nm, which are merging to one broad band at 560 nm with elevated temperature. The bimetallic Ag^{I}/Zn^{II} compound **7** has its maxima at 445 nm with a shoulder at 490 nm and is strongly blue-shifted by 50 nm compared to **4**. Similar to compound **2**, the Ag^{I}/Cd^{II} complex **8** shows two maxima, one at 480 nm and a more intense one at 525 nm, but in this case the emission is strongly blue-shifted. At room temperature the intensity of the two bands is changed and the new maximum is slightly blue-shifted to 470 nm. The same trend in emission wavelength as seen for compounds **4–6** can be seen for compounds **7** and **8**. The PLE spectra of **2** and **7** resemble their Au^{I} pendants, while **8**, still looking quite similar, has an excitation maximum at 430 nm at 293 K. Similar to the spectra shown in Fig. 7, the spectra of Fig. 8 feature the same redshift for the PLE onsets. Except for the Hg^{II} compound **6**, in which PLE spectra appear more like that of one of the mononuclear compounds [PNacK], **1** and **2**, the coordination of the second metal into the ß-diketiminate scaffold in **4**, **5**, **7** and **8** leads to significant increased excitation at shorter wavelengths as well as strongly blue-shifted emissions. While compounds **4** and **7** are quite similar, the influence of the Ag^{I} core in **8** gives rise to the maximum at 525 nm, thus resembling the curve of the PL spectra of **2**. Overall, it can be said that the Au^{I} containing compounds show a larger Stokes shift than the Ag^{I} compounds, but the latter ones show emission at shorter wavelengths. The PL emission of compounds **3–8** is phosphorescence with decay times of up to hundreds of microseconds (see ESI Fig. S62, S63 and Table S1†). The decay kinetics consist of multiple processes and τ_{eff} had to be derived from up to triexponential fits, with the longest lifetime of 818 µs from Au^{I}/Zn^{II} complex **4**. The decay times strongly depend on the temperature and decrease drastically at room temperature. In this context we realized that upon warming the sample, the process with the long lifetime disappears and the fitting could be achieved with one exponential less.

In a previous publication our group investigated the PL properties of the protonated ligand PNac-H and a range of metal complexes, giving an already wide range variety.[43] The PL spectra of compounds **3–8** in Fig. 7 and Fig. 8 demonstrate that the coordination of the second metal has a significant influence on the photoluminescence properties, thus leading to the conclusion that bimetallic compounds are of great interest for PL emitters. As shown here the emission wavelength can easily be tuned with the variation of the metal composition within the same ligand framework, opening a larger range of possibilities for fine tuning.

Quantum chemical calculations

In Table 2, the metal–metal distances of the optimized and experimentally observed geometries (see Fig. 4 and Fig. 5) are compared. Except for **6**, these distances agree to within 0.05 Å (1–2%). For **6**, however, the computed $Au^{I}\cdots Hg^{II}$ distance is 0.27 Å (8%) larger than that found experimentally. The reason for this discrepancy remains unknown.

For all compounds except [PNacAuCuI] (**3**), we find that the lowest lying singlet excited state shows a large oscillator strength (from 0.16 to 0.48 in the mixed length/velocity representation) and dominates the absorption spectrum at wavelengths of about 300–350 nm. See Fig. S72 to S80 in the ESI.† In all cases, this excitation can be understood as a transition from the highest occupied molecular orbital (HOMO) to the lowest unoccupied molecular orbital (LUMO) of the anionic $[NH\text{-}(CH)_3\text{-}NH]^-$ ligand fragment, influenced by the metal ions. These orbitals are depicted in Fig. 9. The pairs of natural transition orbitals (NTOs)[60] that describe this first excited singlet state are depicted in Table S7 of the ESI.†

For **3**, two almost dark states lie below this HOMO–LUMO excited state of the $[NH\text{-}(CH)_3\text{-}NH]^-$ fragment. Thus, for complex **3**, the first state with significant oscillator strength is the third excited state S_3. We find that for the monometallic compounds **1**, **2**, and **9**, the S_1 state of the Cu^{I} compound **9** is significantly red-shifted with respect to the Au^{I} and Ag^{I} counterparts **1** and **2**. For the bimetallic compounds, we find that the relevant excited singlet states are significantly blue-shifted with respect to the monometallic compounds. This is

Table 2 Metal–metal distances [Å] as obtained at the CAM-B3LYP/def2-SV(P) level in comparison with experimental values

		Coinage metal ion	Halide metal ion	Calc. [Å]	Exptl. [Å]
[PNacAuCuI]	**3**	Au	Cu	2.688	2.634(2)
[PNacAuZnCl$_2$]	**4**	Au	Zn	3.247	3.2088(5)
[PNacAuCdI$_2$]	**5**	Au	Cd	3.417	3.3942(4)
[PNacAuHgCl$_2$]	**6**	Au	Hg	3.514	3.2417(2)
[PNacAgZnCl$_2$]	**7**	Ag	Zn	3.067	3.0941(7)
[PNacAgCdI$_2$]	**8**	Ag	Cd	3.250	3.2077(5)

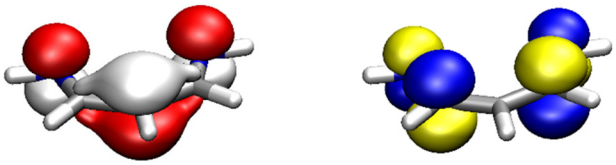

Fig. 9 Highest occupied molecular orbital (HOMO, left) and lowest unoccupied molecular orbital (LUMO, right) as obtained from Hückel molecular-orbital (HMO) theory for the model system $[NH\text{-}(CH)_3\text{-}NH]^-$. Plotted at an isovalue of ± 0.05 bohr$^{-3/2}$.

also observed experimentally, although not so clear for **3** and **6** (Fig. 7).

Furthermore, note that the experimental spectra refer to the solid phase, which renders quantitative comparison with the computed single-molecule (gas-phase) results difficult. The blue-shifts of the bimetallic compounds with respect to the monometallic compounds may be explained by means of a cooperative effect due to the two metal ions. The term "cooperativity" or "cooperative effects" is a well-defined term in computational chemistry. It comprises all effects that go beyond the sum of pair interactions, which are also termed two-body terms. The total energies of molecules, but also other molecular properties such as absorption and emission spectra, can be expanded in a many-body expansion. In this expansion, the one-body contributions comprise the properties of the individual constituents. The two-body contributions comprise the pairwise interactions between the constituents, and the three-body and higher-order contributions define the cooperative effects. In this context, Studer and Grimme *et al.* stated that "cooperative systems require the interplay of at least three functional entities", which was also the point of interest in one of our previously reported publications.[61,62] In the present article, we find that the blue-shifts of the bimetallic compounds with respect to the monometallic compounds may be explained by means of a cooperative effect due to the two metal ions (Table 4). The $[NH\text{-}(CH)_3\text{-}NH]^-$ fragment is one functional entity, and the two metal ions are the other two. The effect of one metal ion on the excited state (band position, intensity) is altered in an indirect manner by metal-to-metal charge transfer from/to the other metal ion. A natural population analysis (NPA)[63] was applied to the unrelaxed difference densities of the singlet excitations of interest (Table 3). It was found that the d-orbital populations of both metal ions were significant, both in the hole density (from which the electron is excited, Table S5†) and in the particle density (to which the electron is excited, Table S6†). The NPA populations also show that the 3d-orbitals of the Cu^I ion play a special role, both in **3** and in **9**. In complex **3**, the Cu 3d-orbital population is as large as 0.273 in the hole density, and the corresponding value for **9** is 0.185. These values are much larger than for all of the other d populations. Also somewhat special are the Au 6p-orbital population (0.058) in the particle density of **3** and the Hg 6s-orbital population (0.040, see Table S6†) in the particle density of **6**. The four compounds with Zn^{II} and Cd^{II} are all very similar and show no peculiarities. This is in accord with the observed spectra shown in Fig. 7 and 8 for these four compounds.

The equilibrium geometries were also optimised for all of the complexes in their first excited triplet state (T_1), which was approximated by a single Kohn–Sham determinant with two

Table 3 Natural population analysis (NPA) of the hole and particle contributions to the unrelaxed difference density of the singlet excited state S_n, as obtained at the CAM-B3LYP/def2-SVPD//CAM-B3LYP/def2-SV(P) level. Displayed are the populations of the p and d shells of the coinage ions (Cu/Ag/Au) and of the metal ions of the metal halides (Cu/Zn/Cd/Hg)

	Hole density				Particle density			
	Cu/Ag/Au		Cu/Zn/Cd/Hg		Cu/Ag/Au		Cu/Zn/Cd/Hg	
	p	d	p	d	p	d	p	d
1	0.002	0.002	—	—	0.010	0.026	—	—
2	0.002	0.010	—	—	0.017	0.028	—	—
3	0.001	0.002	0.028	0.273	0.058	0.013	0.004	0.020
4	0.003	0.007	0.002	0.006	0.007	0.016	0.019	0.004
5	0.003	0.007	0.003	0.005	0.006	0.017	0.028	0.005
6	0.003	0.006	0.003	0.011	0.005	0.017	0.029	0.008
7	0.004	0.005	0.002	0.006	0.007	0.022	0.023	0.004
8	0.003	0.004	0.003	0.005	0.005	0.021	0.034	0.004
9	0.018	0.185	—	—	0.014	0.018	—	—

Table 4 Emission wavelength [nm] with respect to the 0–0 transition between the S_0 ground state and the first excited T_1 state, as obtained at the CAM-B3LYP/def2-SVPD//CAM-B3LYP/def2-SV(P) level

	1	2	3	4	5	6	7	8	9
[nm]	531.3	539.7	560.2	485.1	487.3	489.7	483.7	487.6	655.3

unpaired electrons. With the harmonic vibrational frequencies available for the S_0 and T_1 states, the wavelength of the 0–0 transition was computed from the difference between the respective zero-point-energy corrected DFT total energies. The calculated emission wavelengths listed in Table 4 show a deviation from the experimental measurement for monometallic Au^I and bimetallic Au^I/Hg^{II} compounds **1** and **6**. The calculated emission wavelengths differ by around 100 nm for both. The other calculated values match rather well with the experimental values obtained at room temperature, only differing around 15 nm to 20 nm.

Summary

We presented a synthetic protocol to achieve a series of heterobimetallic compounds comprising a coinage metal (Ag^I or Au^I) and a group 12 metal. The use of the monoanionic bisphosphine-ß-diketiminate ligand (PNac) resembles the principle of orthogonal ligand design and can be used as a building block for such bimetallic systems in an intraligand manner. The target complexes can be either obtained in a step-wise synthetic protocol starting from either the mononuclear Ag^I or Au^I compounds or in a one-pot synthesis with a remarkable cooperative deprotonation step of the ligand. We observed that the presence of two different metals within the same ligand scaffold has a significant influence on the photoluminescence properties. Despite the fact that there is no significant interaction between the metal atoms in compounds **4–8**, the presence of both metals within the same ligand framework led to a change in photoluminescence properties and thus can be attributed to a cooperative activation of the PL properties. The metallophilic interaction between Au^I and Cu^I leads to the strongest increase of room temperature emission compared to the emission at 77 K. Overall, it can be noted that the Au^I containing compounds show a larger Stokes shift than the Ag^I compounds. Going down the group 12 metals from Zn to Hg, an increase in emission wavelength can be observed. To further shed light on these observations, quantum chemical calculations were performed. A significant blue-shift of the relevant excited singlet states was found for the bimetallic compounds in comparison to the monometallic species. The excitation is mostly centred on the ß-diketiminate scaffold, showing intraligand processes. Consequently, the complexation of additional metals at the ß-diketiminate scaffold has a great influence on the PL properties, due to the simultaneous interaction of both metals with the ligand. Our investigation thus clearly shows that PL properties can be tuned by a rational design of heterobimetallic complexes.

Author contributions

F. K. performed the synthesis and characterisation and analysed the data with the help of X. S. and C. Z. D. F. and X. S. assisted with the X-ray diffraction analyses. W. K. performed the quantum chemical calculations. P. W. R. conceived the idea and supervised the work. All authors provided suggestions and comments on the manuscript.

Conflicts of interest

There are no conflicts to declare.

Acknowledgements

The authors are grateful to Deutsche Forschungsgemeinschaft (DFG) for financial support through the Transregional Collaborative Research Centre CRC/TRR 88 “Cooperative Effects in Homo- and Heterometallic Complexes (3MET)” (Projects C1 and C3).

References

1 S. Liu, A. Motta, A. R. Mouat, M. Delferro and T. J. Marks, Very Large Cooperative Effects in Heterobimetallic Titanium-Chromium Catalysts for Ethylene Polymerization/Copolymerization, *J. Am. Chem. Soc.*, 2014, **136**, 10460–10469.

2 D. C. Powers, B. L. Anderson, S. J. Hwang, T. M. Powers, L. M. Pérez, M. B. Hall, S.-L. Zheng, Y.-S. Chen and D. G. Nocera, Photocrystallographic Observation of Halide-Bridged Intermediates in Halogen Photoeliminations, *J. Am. Chem. Soc.*, 2014, **136**, 15346–15355.

3 M. K. Rong, F. Holtrop, J. C. Slootweg and K. Lammertsma, Enlightening developments in 1,3-P,N-ligand-stabilized multinuclear complexes: A shift from catalysis to photoluminescence, *Coord. Chem. Rev.*, 2019, **382**, 57–68.

4 C. Creutz, Mixed Valence Complexes of d^5-d^6 Metal Centers, *Prog. Inorg. Chem.*, 1983, 1–73.

5 M. D. Ward, Metal-metal interactions in binuclear complexes exhibiting mixed valency; molecular wires and switches, *Chem. Soc. Rev.*, 1995, **24**, 121–134.

6 D. E. Richardson and H. Taube, Mixed-valence molecules: Electronic delocalization and stabilization, *Coord. Chem. Rev.*, 1984, **60**, 107–129.

7 V. Balzani, A. Juris, M. Venturi, S. Campagna and S. Serroni, Luminescent and Redox-Active Polynuclear Transition Metal Complexes, *Chem. Rev.*, 1996, **96**, 759–834.

8 C.-M. Che and S.-W. Lai, Structural and spectroscopic evidence for weak metal–metal interactions and metal–substrate exciplex formations in d^{10} metal complexes, *Coord. Chem. Rev.*, 2005, **249**, 1296–1309.

9 J. Campos, Bimetallic cooperation across the periodic table, *Nat. Rev. Chem.*, 2020, **4**, 696–702.

10 V. J. Catalano and S. J. Horner, Luminescent Gold(I) and Silver(I) Complexes of 2-(Diphenylphosphino)-1-methylimidazole (dpim): Characterization of a Three-Coordinate Au(I)–Ag(I) Dimer with a Short Metal–Metal Separation, *Inorg. Chem.*, 2003, **42**, 8430–8438.

11 C. Uhlmann, T. J. Feuerstein, T. P. Seifert, A. P. Jung, M. T. Gamer, R. Köppe, S. Lebedkin, M. M. Kappes and P. W. Roesky, Luminescent early-late-hetero-tetranuclear group IV – Au(I) bisamidinate complexes, *Dalton Trans.*, 2022, **51**, 10357–10360.

12 E. Mas-Marzá, J. A. Mata and E. Peris, Triazolediylidenes: A Versatile Class of Ligands for the Preparation of Discrete Molecules of Homo- and Hetero-Binuclear Complexes for Improved Catalytic Applications, *Angew. Chem., Int. Ed.*, 2007, **46**, 3729–3731.

13 A. Zanardi, J. A. Mata and E. Peris, Palladium Complexes with Triazolyldiylidene. Structural Features and Catalytic Applications, *Organometallics*, 2009, **28**, 1480–1483.

14 A. Zanardi, R. Corberán, J. A. Mata and E. Peris, Homo- and Heterodinuclear Complexes with Triazolyl-diylidene. An Easy Approach to Tandem Catalysts, *Organometallics*, 2008, **27**, 3570–3576.

15 J. A. Mata, F. E. Hahn and E. Peris, Heterometallic complexes, tandem catalysis and catalytic cooperativity, *Chem. Sci.*, 2014, **5**, 1723–1732.

16 A. Zanardi, J. A. Mata and E. Peris, Domino Approach to Benzofurans by the Sequential Sonogashira/Hydroalkoxylation Couplings Catalyzed by New N-Heterocyclic-Carbene-Palladium Complexes, *Organometallics*, 2009, **28**, 4335–4339.

17 K. Uemura and R. Miyake, Paramagnetic One-Dimensional Chain Complex Consisting of Three Kinds of Metallic Species Showing Magnetic Interaction through Metal–Metal Bonds, *Inorg. Chem.*, 2020, **59**, 1692–1701.

18 P. Pyykkö, Strong closed-shell interactions in inorganic chemistry, *Chem. Rev.*, 1997, **97**, 597–636.

19 P. Aguirre-Etcheverry and D. O'Hare, Electronic Communication through Unsaturated Hydrocarbon Bridges in Homobimetallic Organometallic Complexes, *Chem. Rev.*, 2010, **110**, 4839–4864.

20 A. Ceccon, S. Santi, L. Orian and A. Bisello, Electronic communication in heterobinuclear organometallic complexes through unsaturated hydrocarbon bridges, *Coord. Chem. Rev.*, 2004, **248**, 683–724.

21 S. Bestgen, M. T. Gamer, S. Lebedkin, M. M. Kappes and P. W. Roesky, Di- and Trinuclear Gold Complexes of Diphenylphosphinoethyl-Functionalised Imidazolium Salts and their N-Heterocyclic Carbenes: Synthesis and Photophysical Properties, *Chem. – Eur. J.*, 2015, **21**, 601–614.

22 G. J. Rowlands, Ambifunctional cooperative catalysts, *Tetrahedron*, 2001, **10**, 1865–1882.

23 R. Maity, B. S. Birenheide, F. Breher and B. Sarkar, Cooperative Effects in Multimetallic Complexes Applied in Catalysis, *ChemCatChem*, 2021, **13**, 2337–2370.

24 J. H. Ho, S. W. Choy, S. A. Macgregor and B. A. Messerle, Cooperativity in bimetallic dihydroalkoxylation catalysts built on aromatic scaffolds: Significant rate enhancements with a rigid anthracene scaffold, *Organometallics*, 2011, **30**, 5978–5984.

25 S. W. Choy, M. J. Page, M. Bhadbhade and B. A. Messerle, Cooperative catalysis: large rate enhancements with bimetallic rhodium complexes, *Organometallics*, 2013, **32**, 4726–4729.

26 R. L. White-Morris, M. M. Olmstead and A. L. Balch, Aurophilic Interactions in Cationic Gold Complexes with Two Isocyanide Ligands. Polymorphic Yellow and Colorless Forms of $[(\text{Cyclohexyl Isocyanide})_2\text{Au}^{\text{I}}](\text{PF}_6)$ with Distinct Luminescence, *J. Am. Chem. Soc.*, 2003, **125**, 1033–1040.

27 V. W.-W. Yam and E. C.-C. Cheng, in *Photochemistry and photophysics of coordination compounds II*, ed. V. Balzani and S. Campagna, Springer, Berlin, Heidelberg, 2007, pp. 269–309.

28 H. Schmidbaur and A. Schier, Argentophilic Interactions, *Angew. Chem., Int. Ed.*, 2015, **54**, 746–784.

29 M. Mońka, I. E. Serdiuk, K. Kozakiewicz, E. Hoffman, J. Szumilas, A. Kubicki, S. Y. Park and P. Bojarski, Understanding the internal heavy-atom effect on thermally activated delayed fluorescence: application of Arrhenius and Marcus theories for spin–orbit coupling analysis, *J. Mater. Chem. C*, 2022, **10**, 7925–7934.

30 I. O. Koshevoy, Y.-C. Chang, A. J. Karttunen, M. Haukka, T. Pakkanen and P.-T. Chou, Modulation of Metallophilic Bonds: Solvent-Induced Isomerization and Luminescence Vapochromism of a Polymorphic Au–Cu Cluster, *J. Am. Chem. Soc.*, 2012, **134**, 6564–6567.

31 V. W.-W. Yam, V. K.-M. Au and S. Y.-L. Leung, Light-Emitting Self-Assembled Materials Based on d^8 and d^{10} Transition Metal Complexes, *Chem. Rev.*, 2015, **115**, 7589–7728.

32 M. A. Malwitz, S. H. Lim, R. L. White-Morris, D. M. Pham, M. M. Olmstead and A. L. Balch, Crystallization and Interconversions of Vapor-Sensitive, Luminescent Polymorphs of $[(C_6H_{11}NC)_2\text{Au}^{\text{I}}](\text{AsF}_6)$ and $[(C_6H_{11}NC)_2\text{Au}^{\text{I}}](\text{PF}_6)$, *J. Am. Chem. Soc.*, 2012, **134**, 10885–10893.

33 W.-H. Chan, K.-K. Cheung, T. C. Mak and C.-M. Che, Gold(I) complex of 7-diphenylphosphino-2, 4-dimethyl-1, 8-naphthyridine (dpnapy) as a metalloligand for encapsulation of metal ions. Crystal structures of $[\text{AuCu}(\text{dpnapy})_3][\text{ClO}_4]_2$ and $[\text{AuCd}(\text{dpnapy})_3][\text{ClO}_4]_3$, *J. Chem. Soc., Dalton Trans.*, 1998, 873–874.

34 V. R. Naina, F. Krätschmer and P. W. Roesky, Selective coordination of coinage metals using orthogonal ligand scaffolds, *Chem. Commun.*, 2022, **58**, 5332–5346.

35 R. G. Pearson, Hard and soft acids and bases, HSAB, part II: Underlying theories, *J. Chem. Educ.*, 1968, **45**, 643.

36 R. G. Pearson, The HSAB Principle—more quantitative aspects, *Inorg. Chim. Acta*, 1995, **240**, 93–98.

37 M. Dahlen, T. P. Seifert, S. Lebedkin, M. T. Gamer, M. M. Kappes and P. W. Roesky, Tetra- and hexanuclear string complexes of the coinage metals, *Chem. Commun.*, 2021, **57**, 13146–13149.

38 M. Dahlen, E. H. Hollesen, M. Kehry, M. T. Gamer, S. Lebedkin, D. Schooss, M. M. Kappes, W. Klopper and P. W. Roesky, Bright Luminescence in Three Phases—A Combined Synthetic, Spectroscopic and Theoretical Approach, *Angew. Chem.*, 2021, **133**, 23553–23560.

39 M. Dahlen, M. Kehry, S. Lebedkin, M. M. Kappes, W. Klopper and P. W. Roesky, Bi- and trinuclear coinage metal complexes of a PNNP ligand featuring metallophilic interactions and an unusual charge separation, *Dalton Trans.*, 2021, **50**, 13412–13420.

40 C. Kaub, S. Lebedkin, S. Bestgen, R. Köppe, M. M. Kappes and P. W. Roesky, Defined tetranuclear coinage metal chains, *Chem. Commun.*, 2017, **53**, 9578–9581.

41 C. Kaub, S. Lebedkin, A. Li, S. V. Kruppa, P. H. Strebert, M. M. Kappes, C. Riehn and P. W. Roesky, Bimetallic d(10) -Metal Complexes of a Bipyridine Substituted N-Heterocyclic Carbene, *Chem. – Eur. J.*, 2018, **24**, 6094–6104.

42 S. Bestgen, M. Mehta, T. C. Johnstone, P. W. Roesky and J. M. Goicoechea, A "Push–Pull" Stabilized Phosphinidene Supported by a Phosphine–Functionalized β–Diketiminato Ligand, *Chem. – Eur. J.*, 2020, **26**, 9024–9031.

43 C. Zovko, S. Bestgen, C. Schoo, A. Görner, J. M. Goicoechea and P. W. Roesky, A Phosphine Functionalized β–Diketimine Ligand for the Synthesis of Manifold Metal Complexes, *Chem. – Eur. J.*, 2020, **26**, 13191–13202.

44 C. Zovko, F. Krätschmer, S. Schmidt, T. P. Seifert, M. T. Gamer and P. W. Roesky, A Phosphine-ß-diketiminate Nickel(I)-Complex for Small Molecule Activation, *ChemPlusChem*, 2022, **87**, e202200288.

45 F. Krätschmer, *Synthese von multinuklearen mono- und bimetallischen Verbindungen der Münzmetalle sowie die Untersuchung von Metall-Metall Wechselwirkungen auf photophysikalische Eigenschaften*, Cuvillier Verlag, 2023.

46 F. Krätschmer, X. Gui, M. T. Gamer, W. Klopper and P. W. Roesky, Systematic investigation of the influence of electronic substituents on dinuclear gold(I) amidinates: synthesis, characterisation and photoluminescence studies, *Dalton Trans.*, 2022, **51**, 5471–5479.

47 N. Savjani, M. Schormann and M. Bochmann, Structural variation in gold(I)-chelate systems: Synthesis of an asymmetrically bridged β-diketiminato complex of gold, *Polyhedron*, 2012, **38**, 137–140.

48 M. C. Gimeno and A. Laguna, Three- and Four-Coordinate Gold(I) Complexes, *Chem. Rev.*, 1997, **97**, 511–522.

49 I. O. Koshevoy, J. R. Shakirova, A. S. Melnikov, M. Haukka, S. P. Tunik and T. A. Pakkanen, Coinage metal complexes of 2-diphenylphosphino-3-methylindole, *Dalton Trans.*, 2011, **40**, 7927.

50 K. Chen and V. J. Catalano, Luminescent Thermochromism in a Gold(I)–Copper(I) Phosphine–Pyridine Complex, *Eur. J. Inorg. Chem.*, 2015, 5254–5261.

51 R. D. Shannon, Revised effective ionic radii and systematic studies of interatomic distances in halides and chalcogenides, *Acta Crystallogr., Sect. A: Cryst. Phys., Diffr., Theor. Gen. Crystallogr.*, 1976, **32**, 751–767.

52 J. M. López-De-Luzuriaga, M. Monge, M. E. Olmos and D. Pascual, Study of the Nature of Closed-Shell $Hg^{II}\cdots M^{I}$ (M = Cu, Ag, Au) Interactions, *Organometallics*, 2015, **34**, 3029–3038.

53 S. Wang and J. P. Fackler Jr., Structure of bis(μ-methylenediphenylthiophosphinato)-gold(I)mercury(II) bis(1,1-dicyanoethylene-2,2-dithiolato-S,S')aurate, *Acta Crystallogr., Sect. C: Cryst. Struct. Commun.*, 1990, **46**, 2253–2255.

54 S. Wang and J. P. Fackler Jr., Organobimetallic complexes with $Hg[CH^2P(S)Ph_2]_2$. Syntheses and characterization of two structural isomers of $[HgAu(CH_2P(S)Ph_2)_2]PF_6$ and the mercury precursor, *Organometallics*, 1988, 2415–2417.

55 S. Raju, H. B. Singh and R. J. Butcher, Metallophilic interactions: observations of the shortest metallophilicinteractions between closed shell ($d^{10}\cdots d^{10}$, $d^{10}\cdots d^{8}$, $d^{8}\cdots d^{8}$ metal ions [M⋯M′ M = Hg(II) and Pd(II), *Dalton Trans.*, 2020, **49**, 9099–9117.

56 J. M. López-De-Luzuriaga, M. Monge, M. E. Olmos and D. Pascual, Experimental and Theoretical Comparison of the Metallophilicity between d^{10}–d^{10} Au^{I}–Hg^{II} and d^{8}–d^{10} Au^{III}–Hg^{II} Interactions, *Inorg. Chem.*, 2014, **53**, 1275–1277.

57 J. López-De-Luzuriaga, M. Monge, M. Olmos and D. Pascual, $[AuHg(o\text{-}C_6H_4PPh_2)_2I]$: A Dinuclear Heterometallic Blue Emitter, *Inorganics*, 2015, **3**, 27–39.

58 E. Hupf, E. Lork, S. Mebs and J. Beckmann, 6-Diphenylphosphinoacenaphth-5-yl-mercurials as Ligands for d^{10} Metals. Observation of Closed-Shell Interactions of the Type Hg(II)⋯M; M = Hg(II), Ag(I), Au(I), *Inorg. Chem.*, 2015, **54**, 1847–1859.

59 C. Zovko, *Synthese und Charakterisierung unterschiedlicher N, P-Ligandensysteme und deren Metallkomplexe sowie die Untersuchung ihrer photophysikalischen Eigenschaften*, Cuvillier Verlag, 2022.

60 R. L. Martin, Natural transition orbitals, *J. Chem. Phys.*, 2003, **118**, 4775–4777.

61 L. Tebben, C. Mück-Lichtenfeld, G. Fernández, S. Grimme and A. Studer, From Additivity to Cooperativity in Chemistry: Can Cooperativity Be Measured?, *Chem. – Eur. J.*, 2017, **23**, 5864–5873.

62 J. Chmela, M. E. Harding, D. Matioszek, C. E. Anson, F. Breher and W. Klopper, Differential Many-Body Cooperativity in Electronic Spectra of Oligonuclear Transition-Metal Complexes, *ChemPhysChem*, 2016, **17**, 37–45.

63 A. E. Reed, R. B. Weinstock and F. Weinhold, Natural population analysis, *J. Chem. Phys.*, 1985, **83**, 735–746.

